Polarized Optical Spectra, Transition Line Strengths, and the Electronic Energy-Level Structure of $Eu(dpa)_3^{3-}$ Complexes in Single Crystals of Hexagonal $Na_3[Yb_{0.95}Eu_{0.05}(dpa)_3]\cdot NaClO_4\cdot 10H_2O$†

Todd A. Hopkins, James P. Bolender, David H. Metcalf, and F. S. Richardson*

Department of Chemistry, University of Virginia, Charlottesville, Virginia 22901

Received November 30, 1995⊗

Polarized optical absorption and emission measurements are used to locate and assign 52 crystal-field energy levels split out of the $4f^6$ electronic configuration of Eu^{3+} in single crystals of $Na_3[Yb_{0.95}Eu_{0.05}(dpa)_3]\cdot NaClO_4\cdot 10H_2O$ (where dpa ≡ dipicolinate dianion ≡ 2,6-pyridinedicarboxylate). In these crystals, each Eu^{3+} is coordinated to three dipicolinate (dpa) ligands, and the tris-terdentate $Eu(dpa)_3^{3-}$ chelate structures have trigonal-dihedral (D_3) symmetry. The combined optical absorption and emission measurements provide access to the energy-level structures of 27 different $4f^6[SL]J$ multiplet manifolds of Eu^{3+}, and 21 of these multiplet manifolds are represented among the 52 crystal-field levels that are characterized with respect to both location (energy) and symmetry properties. The energy-level data obtained from experiment are analyzed in terms of a model Hamiltonian that includes consideration of both isotropic and nonisotropic 4f-electron/crystal-field interactions. A parametrized form of this Hamiltonian is used to perform parametric fits of calculated-to-experimental energy-level data, and the results obtained from these data fits show a root mean square (rms) deviation of 9.8 cm^{-1} between calculated and observed energies. The Hamiltonian parameters evaluated from the energy-level analyses provide information about both the anisotropies and the overall strength of the 4f-electron/crystal-field interactions that contribute to the energy-level structure of $Eu(dpa)_3^{3-}$ complexes. In addition to energy-level data, the absorption measurements performed in this study permit the quantitative determination of relative optical line strengths for 22 different Stark-level-to-Stark-level transitions observed in the low-temperature axial absorption spectra of $Eu(dpa)_3^{3-}$ in $Na_3[Yb_{0.95}Eu_{0.05}(dpa)_3]\cdot NaClO_4\cdot 10H_2O$.

Introduction

The tris-terdentate coordination complexes formed by the chelation of three dipicolinate (dpa) ligands to a trivalent lanthanide ion (Ln^{3+}) have been used extensively as both optical and magnetic probes in a wide variety of chemical and biochemical studies. Among these complexes, the two most frequently used as optical probes are $Eu(dpa)_3^{3-}$ and $Tb(dpa)_3^{3-}$, each of which exhibits a luminescence that can be excited with high quantum efficiency *and* shows excitation and emission spectra that are particularly sensitive to environmental perturbations. The luminescence properties of $Eu(dpa)_3^{3-}$ and $Tb(dpa)_3^{3-}$ complexes have been investigated, in both crystalline and solution media, by a number of workers.[1−4] The emission spectra obtained from these investigations provide considerable information about energy-level structure within the ^7F_J multiplet manifolds of the $4f^6(Eu^{3+})$ and $4f^8(Tb^{3+})$ electronic configurations in the respective complexes, but the available information falls far short of that needed to support a meaningful crystal-field analysis of $4f^N(Ln^{3+})$ energy-level structure. This situation may be contrasted to that for the structurally similar $Eu(oda)_3^{3-}$ and $Tb(oda)_3^{3-}$ complexes (where oda ≡ oxydiacetate), for which there exist extensive and detailed characterizations and analyses of $4f^N(Ln^{3+})$ energy-level structure and $4f \rightarrow 4f$ transition properties.[5−8] Details of the electronic state structure in $Eu(dpa)_3^{3-}$ and $Tb(dpa)_3^{3-}$ are directly relevant to recent applications of these complexes as optical probes of intermolecular chiral recognition processes in solution.[9−19] In these applications, the $Eu(dpa)_3^{3-}$ and $Tb(dpa)_3^{3-}$ complexes function as energy donors in intermolecular electronic energy-transfer processes, and the efficiencies with which they play that role depend, in large part, on the details of their electronic-state structure (relative to that of the energy acceptors being

* Author to whom correspondence should be addressed.

† dpa ≡ dipicolinate dianion (2,6-pyridinedicarboxylate).

⊗ Abstract published in *Advance ACS Abstracts,* August 1, 1996.

(1) Foster, D. R.; Richardson, F. S. *Inorg. Chem.* **1983**, *22*, 3996.
(2) (a) Murray, G. M.; Sarrio, R. V.; Peterson, J. R. *Inorg. Chim. Acta* **1990**, *176*, 233. (b) Murray, G. M.; Sarrio, R. V.; Peterson, J. R. *Appl. Spectrosc.* **1990**, *44*, 1647. (c) Stump N. A.; Pesterfield, L. L.; Schweitzer, G. K.; Peterson, J. R. *J. Alloys Compd.* **1992**, *180*, 141. (d) Stump N. A.; Pesterfield, L. L.; Schweitzer, G. K.; Peterson, J. R.; Murray, G. M. *Spectrosc. Lett.* **1992**, *25*, 1421.
(3) Bolender, J. P.; Metcalf, D. H.; Richardson, F. S. *J. Alloys Compd.* **1992**, *180*, 177.
(4) Meskers, S. C. J.; Riehl, J. P.; Dekkers, H. P. J. M. *Chem. Phys. Lett.* **1993**, *216*, 241.
(5) Berry, M. T.; Schwieters, C.; Richardson, F. S. *Chem. Phys.* **1988**, *122*, 105.
(6) Berry, M. T.; Schwieters, C.; Richardson, F. S. *Chem. Phys.* **1988**, *122*, 125.
(7) Morley, J. P.; Saxe, J. D.; Richardson, F. S. *Mol. Phys.* **1982**, *47*, 379.
(8) Saxe, J. D.; Morley, J. P.; Richardson, F. S. *Mol. Phys.* **1982**, *47*, 407.
(9) Richardson, F. S.; Metcalf, D. H.; Glover, D. P. *J. Phys. Chem.* **1991**, *95*, 6249.
(10) Metcalf, D. H.; Snyder, S. W.; Demas, J. N.; Richardson, F. S. *J. Am. Chem. Soc.* **1990**, *112*, 5681.
(11) Metcalf, D. H.; Snyder, S. W.; Demas, J. N.; Richardson, F. S. *J. Phys. Chem.* **1990**, *94*, 7143.
(12) Metcalf, D. H.; Stewart, J. M.; Snyder, S. W.; Grisham, C. M.; Richardson, F. S. *Inorg. Chem.* **1992**, *31*, 2445.
(13) Rexwinkel, R. B.; Meskers, S. C. J.; Riehl, J. P.; Dekkers, H. P. J. M. *J. Phys. Chem.* **1992**, *96*, 1112.
(14) Rexwinkel, R. B.; Meskers, S. C. J.; Riehl, J. P.; Dekkers, H. P. J. M. *J. Phys. Chem.* **1992**, *96*, 5725.
(15) Rexwinkel, R. B.; Meskers, S. C. J.; Riehl, J. P.; Dekkers, H. P. J. M. *J. Phys. Chem.* **1993**, *97*, 3875.
(16) Rexwinkel, R. B.; Meskers, S. C. J.; Riehl, J. P.; Dekkers, H. P. J. M. *J. Phys. Chem.* **1993**, *97*, 13519.
(17) Metcalf, D. H.; Bolender, J. P.; Driver, M. S.; Richardson, F. S. *J. Phys. Chem.* **1993**, *97*, 553.
(18) Bolender, J. P.; Metcalf, D. H.; Richardson, F. S. *Chem. Phys. Lett.* **1993**, *213*, 131.
(19) Glover-Fischer, D. P.; Metcalf, D. H.; Bolender, J. P.; Richardson, F. S. *Chem. Phys.* **1995**, *198*, 207.

S0020-1669(95)01524-2 CCC: $12.00

investigated).[19] A more precise knowledge of $Eu(dpa)_3^{3-}$ and $Tb(dpa)_3^{3-}$ energy-level structures is needed to advance these applications beyond their current level of utility.

In the present study, we focus on the measurement and analysis of electronic energy-level structure in $Eu(dpa)_3^{3-}$ complexes. Optical absorption and emission measurements are reported for these complexes in single crystals of hexagonal $Na_3[Yb_{0.95}Eu_{0.05}(dpa)_3]\cdot NaClO_4\cdot 10H_2O$, and the results obtained from these measurements are compared to results obtained from optical excitation and emission measurements on $Eu(dpa)_3^{3-}$ in aqueous solution. The measurements performed on the single-crystal samples provide access to the energy-level structures of 27 different $4f^6[SL]J$ multiplet manifolds of Eu^{3+}, and from these measurements a total of 52 crystal-field (Stark) levels are both located and assigned. These energy-level data are then analyzed in terms of a model Hamiltonian constructed to represent the $4f^6$ electronic state structure of Eu^{3+} in $Eu(dpa)_3^{3-}$, and the results obtained from this analysis provide information about crystal-field interaction strengths, anisotropies, and state vectors. Additionally, the single-crystal absorption spectra are sufficiently well-resolved to permit the quantitative determination of relative optical line strengths for transitions between individual crystal-field levels of Eu^{3+} in hexagonal $Na_3[Yb_{0.95}Eu_{0.05}(dpa)_3]\cdot NaClO_4\cdot 10H_2O$.

Albertsson has reported single-crystal X-ray diffraction studies on a series of compounds that contain $Ln(dpa)_3^{3-}$ complexes, including hexagonal $Na_3[Yb(dpa)_3]\cdot NaClO_4\cdot 10H_2O$.[20−23] These studies show that the $Ln(dpa)_3^{3-}$ complexes have tris-terdentate chelate structures in which each dpa ligand is coordinated to the Ln^{3+} ion via two carboxylate oxygen donor atoms and a pyridyl nitrogen atom. The LnO_6N_3 coordination polyhedron has a slightly distorted tricapped trigonal prism structure in which oxygen atoms are located at the apices of the trigonal prism and nitrogen atoms are in the capping positions. Each of the three bicyclic chelate rings in a $Ln(dpa)_3^{3-}$ complex has a 2-fold symmetry axis that coincides with a Ln−N coordination axis, and taken together, the chelate rings form a three-bladed propeller-like structure of trigonal-dihedral (D_3) symmetry. This structure is chiral, with a handedness that reflects the screw sense (or helicity) of the three-bladed propeller assembly. Complexes in which the propeller assembly has a *left-handed* screw sense (about its 3-fold symmetry axis) are generally labeled as Λ, and those in which the propeller assembly has a *right-handed* screw sense are generally labeled as Δ. In solution, $Ln(dpa)_3^{3-}$ complexes exist as a racemic mixture of rapidly interconverting Λ-$Ln(dpa)_3^{3-}$ and Δ-$Ln(dpa)_3^{3-}$ enantiomers,[24] and they also crystallize as racemates. Structural representations of the Λ and Δ enantiomeric forms of a $Ln(dpa)_3^{3-}$ complex are shown in Figure 1.

In hexagonal $Na_3[Yb(dpa)_3]\cdot NaClO_4\cdot 10H_2O$ (space group $P\bar{6}2c$ with $Z = 2$), the $Yb(dpa)_3^{3-}$ complexes are located in mirror-related layers perpendicular to the crystal *c*-axis, and complexes in adjacent layers are connected via sodium ions and water molecules to form infinite linear chains *along* the crystal *c*-axis.[22] Each $Yb(dpa)_3^{3-}$ structural unit has D_3 point-group symmetry (with its 3-fold symmetry axis aligned parallel to the crystal *c*-axis), but these structural units alternate between Λ and Δ enantiomeric forms along the *c*-axis. Our polarized optical measurements on single crystals of $Na_3[Yb_{0.95}Eu_{0.05}(dpa)_3]\cdot NaClO_4\cdot 10H_2O$ indicate that the structural properties of these crystals are essentially identical with those of $Na_3[Yb(dpa)_3]\cdot NaClO_4\cdot 10H_2O$. Eu^{3+} is larger than Yb^{3+}, but with Eu^{3+}/Yb^{3+} concentration ratios < 0.1, this appears not to produce any significant structural distinctions between $Na_3[Yb(dpa)_3]\cdot NaClO_4\cdot 10H_2O$ and $Na_3[Yb_{1-x}Eu_x(dpa)_3]\cdot NaClO_4\cdot 10H_2O$ ($x < 0.1$).

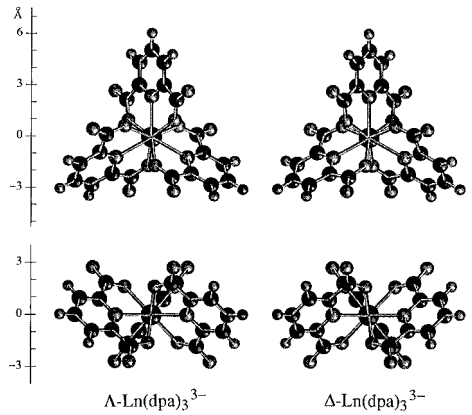

Figure 1. Structural representations of Λ-$Ln(dpa)_3^{3-}$ and Δ-$Ln(dpa)_3^{3-}$ enantiomers. The top structures are viewed along the trigonal (C_3) symmetry axis, and the bottom structures are viewed along one of the digonal (C_2) symmetry axes. The dimensions of the structures are indicated by the angstrom (Å) scales shown on the left-hand side of the figure.

The *chirality-related* optical properties of $Eu(dpa)_3^{3-}$ are of considerable interest, but they are not accessible to study by conventional chiroptical measurement techniques. As was noted above, $Eu(dpa)_3^{3-}$ exists as a racemic mixture of rapidly interconverting Λ-$Eu(dpa)_3^{3-}$ and Δ-$Eu(dpa)_3^{3-}$ enantiomeric structures (optical antipodes) in solution, and it crystallizes as a Λ,Δ-$Eu(dpa)_3^{3-}$ racemate. Therefore, neither solution samples nor crystalline samples of $Eu(dpa)_3^{3-}$ exhibit any circular dichroism or optical rotatory properties under ordinary, equilibrium conditions. However, there are several methods one may use to examine the chiroptical properties of $Eu(dpa)_3^{3-}$ in solution, each of which involves either a static displacement or a dynamic disturbance of the Λ-$Eu(dpa)_3^{3-}$ ⇌ Δ-$Eu(dpa)_3^{3-}$ enantiomer interconversion processes. One method is based on the use of chiral chemical reagents that, when present in solution with $Eu(dpa)_3^{3-}$, will displace the Λ ⇌ Δ equilibrium state away from that of a racemic mixture.[25] These solutions will then exhibit chiroptical properties that may be related to those characteristic of the dominant enantiomer population. A second method is based on the use of circularly polarized light to preferentially excite either Λ or Δ enantiomers and thereby create a nonracemic excited-state population that may be studied via chiroptical luminescence measurement techniques.[24,26,27] Finally, we mention a third method that is directly related to the use of $Eu(dpa)_3^{3-}$ complexes as optical probes of chiral recognition processes in solution. In this method, the solution samples of $Eu(dpa)_3^{3-}$ contain small concentrations of chiral molecules that exhibit enantioselectivity in their quenching of Λ-$Eu(dpa)_3^{3-}$ *versus* Δ-$Eu(dpa)_3^{3-}$ excited-state populations. The $Eu(dpa)_3^{3-}$ complexes are excited with unpolarized light to prepare an initially racemic excited-state population, which then evolves to a nonracemic composition that reflects enanti-

(20) Albertsson, J. *Acta Chem. Scand.* **1970**, *24*, 1213.
(21) Albertsson, J. *Acta Chem. Scand.* **1972**, *26*, 985.
(22) Albertsson, J. *Acta Chem. Scand.* **1972**, *26*, 1005.
(23) Albertsson, J. *Acta Chem. Scand.* **1972**, *26*, 1023.
(24) Metcalf, D. H.; Snyder, S. W.; Demas, J. N.; Richardson, F. S. *J. Am. Chem. Soc.* **1990**, *112*, 469.
(25) (a) Hilmes, G. L.; Coruh, N.; Riehl, J. P. *Inorg. Chem.* **1988**, *27*, 1136. (b) Coruh, N.; Hilmes, G. L.; Riehl, J. P. *Inorg. Chem.* **1988**, *27*, 3647. (c) Wu, S.; Hilmes, G. L.; Riehl, J. P. *J. Phys. Chem.* **1989**, *93*, 2307. (d) Riehl J. P. *Analytical Applications of Circular Dichroism*, Purdie, N.; Brittain, H. G., Eds.; Elsevier: Amsterdam, 1994; pp. 207−239.
(26) Metcalf, D. H.; Richardson, F. S. *J. Alloys Compd.* **1994**, *207/208*, 59.
(27) Richardson, F. S.; Metcalf, D. H. In *Circular Dichroism: Interpretation and Applications*; Nakanishi, K., Berova, N., Woody, R., Eds.; VCH Publishers: New York, 1994; Chapter 7, pp 153−177.

oselective excited-state quenching actions. Chiroptical luminescence measurements are then used to characterize the chiroptical properties of the dominant excited-state population.[19,27]

In the present study we focus primarily on the energy-level structure of $Eu(dpa)_3^{3-}$, as determined from optical absorption and emission measurements performed on single crystals of $Na_3[Yb_{0.95}Eu_{0.05}(dpa)_3]\cdot NaClO_4\cdot 10H_2O$. However, comparisons between solution and crystal spectra are also included.

Experimental Methods

Compound and Crystal Sample Preparation. Hexagonal crystals of $Na_3[Yb_{1-x}Eu_x(dpa)_3]\cdot NaClO_4\cdot 10H_2O$ were grown from aqueous solution following procedures closely similar to those used by Albertsson[22] in the preparation of hexagonal $Na_3[Yb(dpa)_3]\cdot NaClO_4\cdot 10H_2O$. In our case, the mother solution contained 0.95:0.05:3.00 molar ratios of ytterbium perchlorate *to* europium perchlorate *to* disodium dipicolinate, and the pH of the solution was approximately 7.5. Morphologically well-defined hexagonal crystals developed from the solution at room temperature over a period of weeks, and the yield of optical quality crystals was reasonably good. The crystals harvested for optical studies were typically well-formed hexagonal plates of *ca.* 1 mm thickness, which under inspection with a polarizing microscope showed uniaxial symmetry properties. The crystals showed no signs of deterioration during storage under ordinary laboratory atmospheric conditions, and their optical properties remained unchanged over periods of months after their removal from the mother solution.

No attempts were made to determine the exact ratio of Yb^{3+} to Eu^{3+} concentrations in the crystals harvested for optical studies, but comparisons between optical absorbance data obtained on these crystals and on solution samples of known $Eu(dpa)_3^{3-}$ concentrations indicate that the concentration of $Eu(dpa)_3^{3-}$ complexes in the crystals is within ±20% of the 96.2 mM value predicted for crystals of stoichiometric formula $Na_3[Yb_{0.95}Eu_{0.05}(dpa)_3]\cdot NaClO_4\cdot 10H_2O$. This assumes that the (average) unit-cell dimensions in $Na_3[Yb_{0.95}Eu_{0.05}(dpa)_3]\cdot NaClO_4\cdot 10H_2O$ will not be significantly different from those determined for $Na_3[Yb(dpa)_3]\cdot NaClO_4\cdot 10H_2O$.[22] This is a quite reasonable assumption based on the relatively small difference between the ionic radii of Eu^{3+} and Yb^{3+}, which are estimated by Shannon[28] to be approximately 1.12 and 1.04 Å, respectively, in 9-coordinate complexes. It is also compatible with X-ray diffraction results obtained on single crystals of hexagonal $Na_3[Yb_{0.95}Sm_{0.05}(dpa)_3]\cdot NaClO_4\cdot 10H_2O$, which show that the structural parameters of these crystals are essentially identical with those of $Na_3[Yb(dpa)_3]\cdot NaClO_4\cdot 10H_2O$.[29] Hereafter we will use the notation YbEuDPA in referring to the crystal samples examined in the present work and assume that the mole percent ratio of Yb^{3+} to Eu^{3+} ions in these crystals is very close to 95:5.

The single-crystal samples used in our optical absorption and emission experiments were attached to a one-piece copper mount with Crycon grease and indium foil, and the copper mount was attached to the cold head of a closed-cycle helium refrigerator/cryostat, with strips of indium providing a thermally conductive interface. The crystal samples were attached to the copper mount with their unique (optic) axis aligned either parallel or perpendicular to the direction of light propagation in the optical absorption experiments and the direction of excitation and emission detection in the optical emission experiments. Parallel alignment of the unique axis and the direction of light propagation is referred to here as an *axial* orientation. Perpendicular alignment of the unique axis and the direction of light propagation is referred to as an *orthoaxial* orientation.

In our initial optical experiments, the crystal samples were lightly coated with Crycon grease to inhibit their possible deterioration (via efflorescence) under the high-vacuum conditions in the closed-cycle helium refrigerator/cryostat. However, a repeat of these experiments with unprotected crystal samples yielded essentially identical results, and the crystals showed no signs of deterioration during multiple up-and-down temperature changes (between *ca.* 10 and 293 K) in the cryostat.

(28) Shannon, R. D. *Acta Crystallogr., Sect. A* **1976**, *32*, *751*−767.
(29) Bolender, J. P.; Sabat, M. Unpublished results, University of Virginia.

Table 1. Electric (μ) and Magnetic (m) Dipole Selection Rules for Optical Absorption and Emission Measurements on $Eu(dpa)_3^{3-}$ Complexes in Hexagonal $Na_3[Yb_{0.95}Eu_{0.05}(dpa)_3]\cdot NaClO_4\cdot 10H_2O$

		orthoaxial spectra[c]	
transition type[a]	axial spectra[b]	σ-polarized	π-polarized
$A_1 \leftrightarrow A_1$	forbidden	forbidden	forbidden
$A_1 \leftrightarrow A_2$	forbidden	m_0	μ_0
$A_2 \leftrightarrow A_2$	forbidden	forbidden	forbidden
$A_1 \leftrightarrow E$	$\mu_{\pm1}$, $m_{\pm1}$	$\mu_{\pm1}$	$m_{\pm1}$
$A_2 \leftrightarrow E$	$\mu_{\pm1}$, $m_{\pm1}$	$\mu_{\pm1}$	$m_{\pm1}$
$E \leftrightarrow E$	$\mu_{\pm1}$, $m_{\pm1}$	$\mu_{\pm1}$, m_0	μ_0, $m_{\pm1}$

[a] Energy levels are labeled according to their irreducible representation (irrep) in the D_3 point group. [b] Light propagating along the crystallographic *c*-axis (the *unique* axis), which is parallel to the trigonal symmetry axes of the $Eu(dpa)_3^{3-}$ complexes. [c] Light propagating along a direction orthogonal to the crystallographic *c*-axis.

Optical Absorption Measurements on Crystal Samples. All absorption spectra were obtained with a Cary Model 2415 UV−vis−near-IR spectrophotometer. A CTI-Cryogenics closed-cycle helium refrigerator/cryostat, controlled by a Lake Shore Cryotronics temperature controller (Model DRC-70), was used to achieve a cold-head temperature of 10 K. Absorption spectra were recorded over the 300−600 nm wavelength range. Unpolarized axial, and σ- and π-polarized orthoaxial spectra were measured for YbEuDPA crystals. The orthoaxial spectral measurements were taken by fitting a linear polarizing element into the spectrophotometer.

Optical line strengths were determined for 22 of the transitions observed in the axial absorption spectra. These line strengths were determined by integrating observed absorbances over transition line profiles and then evaluating

$$S_{i\rightarrow f}(\alpha) = \frac{3.06 \times 10^{-3} g_i}{X_i(T)\chi_\lambda c_m b}\int_{i\rightarrow f}\frac{A(\bar{\nu})\,d\bar{\nu}}{\bar{\nu}}\,(D^2) \qquad (1)$$

where $S_{i\rightarrow f}(\alpha)$ denotes the unpolarized axial line strength of a transition $i \rightarrow f$, expressed in units of D^2 (D ≡ 1 debye unit = 10^{-18} esu cm = 3.3356×10^{-30} C m); g_i is the degeneracy of level i; $X_i(T)$ is the fractional thermal (Boltzmann) population of level i at the sample temperature (T); c_m is the molar concentration of Eu^{3+} in YbEuDPA; b is the sample thickness (cm); χ_λ is a correction factor for bulk sample refractivity at the transition wavelength λ; $A(\bar{\nu})$ denotes the decadic absorbance of the sample at wavenumber $\bar{\nu}$; and the integration is over the absorbance profile of the $i \rightarrow f$ transition. The molar concentration of Eu^{3+} in YbEuDPA was assumed to be 0.0962 (c_m = 0.0962 mol/L), as discussed earlier in the paper, and all of our unpolarized axial absorption measurements were performed on crystals of 0.3 cm thickness. Refractive index dispersion data for $Na_3[Ln(dpa)_3]\cdot NaClO_4\cdot 10H_2O$ systems are not available, so the χ_λ factors in our line-strength expression could not be evaluated. All of the line-strength data reported in this paper are given in units of 10^{-6} D^2/χ_λ.

The surface temperature of the crystal samples was maintained at 10 K, but analyses of relative line intensities observed in the absorption spectra indicated that the internal temperature of the crystals was *ca.* 20 K. The latter temperature was used in calculating values for the Boltzmann population factors, $X_A(T)$, that appear in eq 1. Integrated areas of absorption lines were determined using computer software. The integration program uses a fitting routine to fit a combination of Gaussian and Lorentzian line shapes to the experimentally observed spectral lines. The program then uses the fitted combination of Gaussian and Lorentzian line shapes to calculate areas.

Optical Emission Measurements on Crystal Samples. Optical emission spectra were measured using instrumentation constructed in this laboratory. An argon-ion laser was used as an excitation source; sample luminescence was dispersed with a 0.75 m double-grating monochromator, and luminescence intensity was measured using photon-counting techniques. In all experiments, sample excitation was along the same direction as emission detection. Two different optical cryostats were used to control sample temperature in the emission experiments. A closed-cycle helium refrigerator was used in experiments carried out at 10 and 293 K, and a liquid-nitrogen-cooled cryostat was used in experiments carried out at 77 K. Single crystals of

Table 2. Calculated and Experimentally Observed Crystal-Field Energy Levels of Eu^{3+} in Hexagonal $Na_3[Yb_{0.95}Eu_{0.05}(dpa)_3]\cdot NaClO_4\cdot 10H_2O$

				energy (cm^{-1})							energy (cm^{-1})		
level no.	term[a]	J[a]	Γ[b]	calcd[c]	expt[d]	Δ[e]	level no.	term[a]	J[a]	Γ[b]	calcd[c]	expt[d]	Δ[e]
1	^{7}F	0	A_1	−1	0	−1	75	^{5}G(3)	6	A_2	26 504	26 506	−2
2	^{7}F	1	A_2	324	322	2	76	^{5}G(3)	4	E	26 510	nd	
3	^{7}F	1	E	402	397	5	77	^{5}G(3)	2	A_1	26 516	nd	
4	^{7}F	2	E	994	985	9	78	^{5}G(3)	4	A_1	26 538	nd	
5	^{7}F	2	A_1	1 019	nd		79	^{5}G(3)	6	E	26 555	26 540	15
6	^{7}F	2	E	1 081	1 082	−1	80	^{5}G(3)	5	A_2	26 556	nd	
7	^{7}F	3	A_2	1 824	1 821	3	81	^{5}G(3)	6	E	26 561	26 563	−2
8	^{7}F	3	E	1 835	nd		82	^{5}G(3)	6	A_1	26 572	nd	
9	^{7}F	3	A_2	1 846	1 864	−18	83	^{5}G(3)	5	E	26 574	26 576	−2
10	^{7}F	3	E	1 925	1 920	5	84	^{5}G(3)	6	E	26 591	nd	
11	^{7}F	3	A_1	1 937	nd		85	^{5}G(3)	5	A_2	26 598	nd	
12	^{7}F	4	E	2 652	2 667	−15	86	^{5}G(3)	4	A_1	26 607	nd	
13	^{7}F	4	A_2	2 803	2 799	4	87	^{5}G(3)	6	E	26 611	nd	
14	^{7}F	4	E	2 840	2 833	7	88	^{5}G(3)	5	E	26 634	nd	
15	^{7}F	4	A_1	2 905	nd		89	^{5}G(3)	4	E	26 644	26 655	−11
16	^{7}F	4	E	3 010	3 006	4	90	^{5}G(3)	3	A_2	26 670	nd	
17	^{7}F	4	A_1	3 076	nd		91	^{5}G(3)	4	A_1	26 690	nd	
18	^{7}F	5	A_2	3 760	3 748	12	92	^{5}G(3)	4	E	26 717	nd	
19	^{7}F	5	E	3 781	3 788	−7	93	^{5}G(3)	3	A_2	26 756	nd	
20	^{7}F	5	E	3 931	3 911	20	94	^{5}L	8	A_1	26 982	nd	
21	^{7}F	5	E	4 015	4 035	−20	95	^{5}L	8	E	27 005	nd	
22	^{7}F	5	E	4 063	4 063	0	96	^{5}L	8	E	27 046	nd	
23	^{7}F	5	A_1	4 064	nd		97	^{5}L	8	E	27 053	nd	
24	^{7}F	5	A_2	4 087	nd		98	^{5}L	8	A_2	27 057	nd	
25	^{7}F	6	A_1	4 948	nd		99	^{5}L	8	A_1	27 064	nd	
26	^{7}F	6	A_2	4 950	4 950	0	100	^{5}L	8	E	27 094	nd	
27	^{7}F	6	E	4 985	nd		101	^{5}L	8	E	27 104	nd	
28	^{7}F	6	E	4 992	5 006	−14	102	^{5}L	8	A_1	27 145	nd	
29	^{7}F	6	A_1	5 012	nd		103	^{5}L	8	E	27 154	nd	
30	^{7}F	6	A_2	5 022	nd		104	^{5}L	8	A_2	27 190	nd	
31	^{7}F	6	E	5 089	5 080	9	105	^{5}D(3)	4	A_1	27 508	nd	
32	^{7}F	6	E	5 144	nd		106	^{5}D(3)	4	E	27 511	27 515	−4
33	^{7}F	6	A_1	5 163	nd		107	^{5}D(3)	4	A_2	27 513	27 511	2
34	^{5}D(3)	0	A_1	17 200	17 191	9	108	^{5}D(3)	4	E	27 554	27 551	3
35	^{5}D(3)	1	A_2	18 927	18 930	−3	109	^{5}D(3)	4	A_1	27 554	nd	
36	^{5}D(3)	1	E	18 951	18 951	0	110	^{5}D(3)	4	E	27 574	27 561	13
37	^{5}D(3)	2	E	21 398	21 397	1	111	^{5}L	9	A_1	27 675	nd	
38	^{5}D(3)	2	A_1	21 400	nd		112	^{5}L	9	E	27 697	nd	
39	^{5}D(3)	2	E	21 418	21 433	−15	113	^{5}L	9	E	27 732	nd	
40	^{5}D(3)	3	A_2	24 242	nd		114	^{5}L	9	A_1	27 745	nd	
41	^{5}D(3)	3	E	24 261	nd		115	^{5}L	9	A_2	27 773	nd	
42	^{5}D(3)	3	A_1	24 278	nd		116	^{5}L	9	A_2	27 794	nd	
43	^{5}D(3)	3	A_2	24 281	nd		117	^{5}L	9	E	27 798	nd	
44	^{5}D(3)	3	E	24 290	nd		118	^{5}L	9	A_1	27 802	nd	
45	^{5}L	6	A_1	24 916	nd		119	^{5}L	9	E	27 818	nd	
46	^{5}L	6	E	24 952	24 930	22	120	^{5}L	9	E	27 836	nd	
47	^{5}L	6	E	25 024	nd		121	^{5}L	9	E	27 863	nd	
48	^{5}L	6	A_1	25 086	nd		122	^{5}L	9	A_2	27 866	nd	
49	^{5}L	6	A_2	25 095	nd		123	^{5}L	9	A_1	27 873	nd	
50	^{5}L	6	E	25 123	nd		124	^{5}L	10	A_1	28 089	nd	
51	^{5}L	6	A_2	25 180	nd		125	^{5}L	10	E	28 109	nd	
52	^{5}L	6	E	25 184	25 189	−5	126	^{5}L	10	E	28 172	nd	
53	^{5}L	6	A_1	25 201	nd		127	^{5}L	10	A_2	28 227	nd	
54	^{5}L	7	E	25 929	25 926	3	128	^{5}L	10	E	28 231	nd	
55	^{5}L	7	A_1	25 963	nd		129	^{5}L	10	A_1	28 238	nd	
56	^{5}L	7	E	25 986	nd		130	^{5}L	10	E	28 259	nd	
57	^{5}L	7	A_2	26 023	26 024	−1	131	^{5}L	10	A_1	28 281	nd	
58	^{5}L	7	E	26 045	26 060	−15	132	^{5}L	10	A_2	28 284	nd	
59	^{5}L	7	A_1	26 048	nd		133	^{5}L	10	E	28 315	nd	
60	^{5}L	7	A_2	26 067	nd		134	^{5}L	10	A_2	28 412	nd	
61	^{5}L	7	E	26 086	nd		135	^{5}L	10	E	28 415	nd	
62	^{5}L	7	A_2	26 142	nd		136	^{5}L	10	E	28 438	nd	
63	^{5}L	7	E	26 160	26 163	−3	137	^{5}L	10	A_1	28 452	nd	
64	^{5}G(3)	3	A_2	26 257	nd		138	^{5}H(1)	3	A_2	30 698	nd	
65	^{5}G(3)	3	A_1	26 295	nd		139	^{5}H(1)	3	E	30 733	nd	
66	^{5}G(3)	3	E	26 307	26 318	−11	140	^{5}H(1)	3	A_1	30 761	nd	
67	^{5}G(3)	2	E	26 340	26 355	−15	141	^{5}H(1)	3	E	30 774	nd	
68	^{5}G(3)	2	E	26 391	26 392	−1	142	^{5}H(1)	7	A_2	30 807	nd	
69	^{5}G(3)	2	E	26 425	nd		143	^{5}H(1)	3	A_2	30 850	nd	
70	^{5}G(3)	2	A_1	26 446	nd		144	^{5}H(1)	7	A_1	30 855	nd	
71	^{5}G(3)	5	E	26 463	nd		145	^{5}H(1)	7	E	30 857	nd	
72	^{5}G(3)	6	A_2	26 476	26 460	16	146	^{5}H(1)	7	E	30 883	nd	
73	^{5}G(3)	6	A_1	26 492	nd		147	^{5}H(1)	7	A_1	30 926	nd	
74	^{5}G(3)	5	E	26 499	26 493	6	148	^{5}H(1)	7	E	30 935	nd	

Table 2 (Continued)

				energy (cm^{-1})							energy (cm^{-1})		
level no.	term[a]	J[a]	Γ[b]	calcd[c]	expt[d]	Δ[e]	level no.	term[a]	J[a]	Γ[b]	calcd[c]	expt[d]	Δ[e]
149	^{5}H(1)	7	A_2	30 956	nd		167	^{5}H(1)	5	A_2	31 434	nd	
150	^{5}H(1)	7	E	30 964	nd		168	^{5}H(1)	6	E	31 447	31 458	−11:11
151	^{5}H(1)	7	E	31 013	nd		169	^{5}H(1)	6	E	31 471	nd	
152	^{5}H(1)	7	A_2	31 051	nd		170	^{5}H(1)	5	A_2	31 486	31 470	16
153	^{5}H(1)	4	E	31 171	31 161	10	171	^{5}H(1)	5	E	31 522	31 520	2
154	^{5}H(1)	4	E	31 188	nd		172	^{5}H(1)	5	E	31 551	nd	
155	^{5}H(1)	4	A_1	31 210	nd		173	^{5}H(1)	6	A_2	31 556	nd	
156	^{5}H(1)	4	A_2	31 211	nd		174	^{5}H(1)	5	A_1	31 564	nd	
157	^{5}H(1)	4	A_1	31 254	nd		175	^{3}P(6)	0	A_1	32 763	nd	
158	^{5}H(1)	4	E	31 275	31 283	−8	176	^{5}F(2)	3	E	32 917	nd	
159	^{5}H(1)	6	E	31 333	nd		177	^{5}F(2)	3	A_1	32 932	nd	
160	^{5}H(1)	6	A_2	31 341	31 353	−12	178	^{5}F(2)	2	E	32 963	nd	
161	^{5}H(1)	6	A_1	31 345	nd		179	^{5}F(2)	2	A_1	32 990	nd	
162	^{5}H(1)	6	E	31 352	nd		180	^{5}F(2)	2	E	33 011	nd	
163	^{5}H(1)	6	A_1	31 364	nd		181	^{5}F(2)	3	A_2	33 036	nd	
164	^{5}H(1)	6	E	31 388	31 386	2	182	^{5}F(2)	3	E	33 115	nd	
165	^{5}H(1)	6	E	31 421	nd		183	^{5}F(2)	3	A_2	33 155	nd	
166	^{5}H(1)	6	A_1	31 425	nd								

[a] Identifies the *principal SLJ* components of the eigenvectors. [b] Irreducible representation (irrep) label in D_3 point group. [c] Calculated by using the Hamiltonian parameter values listed in Table 3. [d] Experimentally determined locations of energy levels, with $1/\lambda$(air) to $1/\lambda$(vacuum) corrections included. Uncertainties in the energy-level locations are ca. ± 3 cm^{-1} (on average). nd ≡ not determined (i.e., energy level not fully characterized with respect to location and/or symmetry type). [e] Difference between calculated and observed energies.

YbEuDPA were mounted with their unique (optic) axis aligned either parallel or perpendicular to the direction of emission detection.

For the hexagonal YbEuDPA crystals examined in this study, emission measured along the crystallographic *c*-axis (i.e., the unique axis) is unpolarized, and no polarizing (or analyzing) optical elements were used in our *axial* emission experiments. However, emission measured along a direction that is *perpendicular* to the crystallographic *c*-axis (as in our orthoaxial spectral measurements) can exhibit at least some degree of linear polarization. In our orthoaxial emission experiments, the sample luminescence was analyzed in terms of intensity components polarized perpendicular (σ) and parallel (π) to the crystal *c*-axis. This was done by using a dynamic photoelastic (polarization) modulator that alternately transmitted σ- and π-polarized luminescence intensities to the emission detection unit of our spectrophotometer. The photoelastic modulator (PEM) was a Hinds International Model PEM-80, operated at a modulation frequency of *ca.* 100 kHz.

All of the luminescence observed in our experiments originates from the $^5D(3)_0$ multiplet level of Eu^{3+} (located at 17 191 cm^{-1} above ground). The energy gap between this multiplet and the next lower-energy multiplet ($^7F_6$) is *ca.* 12 000 cm^{-1}, which is larger than any lattice phonon or molecular vibrational energies in the YbEuDPA crystals. Therefore, nonradiative decay processes for $^5D(3)_0$ are relatively slow, and this multiplet exhibits a reasonably strong luminescence. In this study, we measured luminescence spectra throughout the $^5D(3)_0 \rightarrow {}^7F_J$ (where $J = 0-6$) transition regions. In all cases, the luminescence was excited with the 465.8 nm line of an argon-ion laser, which corresponds to $^7F_0 \rightarrow {}^5D(3)_2$ excitation.

Emission Excitation Spectra. Emission excitation measurements were carried out using instrumentation constructed in this laboratory. A Nd:YAG pumped dye laser (using Coumarin-480, Coumarin-500, and a combination of Rhodamine-590 and −610 as dyes) was used as the excitation source. Sample luminescence was detected using the same instrumentation described for the optical emission measurements. A liquid-nitrogen-cooled cryostat was used to achieve a sample temperature of 77 K. Unpolarized *axial* and linearly (σ- and π-) polarized *orthoaxial* emission excitation spectra were recorded over the 465−585 nm range ($^7F_0 \rightarrow {}^5D(3)_{2,1,0}$ transition regions), with sample luminescence monitored at 617 nm ($^7F_2 \leftarrow {}^5D(3)_0$ transition region).

Data Analysis

Optical Selection Rules and Line Assignments. The crystal-field levels split out of the $4f^6$ electronic configuration of Eu^{3+} in $Eu(dpa)_3^{3-}$ complexes may be classified according to the transformation properties of their state vectors under the symmetry operations of the D_3 point group. These transformation properties are specified by the three irreducible representations (irreps) contained in D_3, which are labeled here as A_1, A_2, and E. We shall use these D_3 irrep labels to identify the symmetry properties of crystal-field states and to classify transitions *between* crystal-field levels into the following six types: $A_1 \leftrightarrow A_1$; $A_1 \leftrightarrow A_2$; $A_2 \leftrightarrow A_2$; $A_1 \leftrightarrow E$; $A_2 \leftrightarrow E$; and $E \leftrightarrow E$. Optical selection rules for each of these transition types depend on the polarization properties of the perturbing radiation field and on the interaction mechanisms responsible for the transitions.

All transitions observed in the optical absorption and emission spectra reported in the present study may be presumed to occur via electric- and/or magnetic-dipole interaction mechanisms, and the relevant interaction operators for connecting crystal-field states are the electric-dipole ($\boldsymbol{\mu}$) and magnetic-dipole ($\mathbf{m}$) moment operators. Here we express these dipole operators in a spherical coordinate basis, $q = 0, \pm 1$, chosen such that for any given $Eu(dpa)_3^{3-}$ complex the $q = 0$ axis is defined to be coincident with the trigonal symmetry axis of the complex. Expressed in this basis, the μ_0 and m_0 components of the $\boldsymbol{\mu}$ and $\mathbf{m}$ operators each transform as the A_2 irrep under the symmetry operations of the D_3 point group, and the $\mu_{\pm 1}$ and $m_{\pm 1}$ components each transform as the E irrep under the symmetry operations of this group. Given these symmetry properties of the μ_q and m_q operator components, electric- and magnetic-dipole selection rules are easily derived for each of the six transition types defined in the preceding paragraph. The selection rules relevant to our optical absorption and emission measurements on single crystals of YbEuDPA are shown in Table 1. Recall that in these crystals each $Eu(dpa)_3^{3-}$ complex is oriented with its trigonal symmetry axis aligned parallel to the crystallographic *c*-axis. For measurements performed on isotropic solution samples of $Eu(dpa)_3^{3-}$, the relevant selection rules are as follows: the $A_1 \leftrightarrow A_1$ and $A_2 \leftrightarrow A_2$ transition types are both electric- and magnetic-dipole *forbidden*, and the remaining four transition types are both electric- and magnetic-dipole *allowed*.

Among the *J*-multiplet-to-*J*-multiplet transition regions examined in this study, only two are expected to exhibit lines that have predominantly *magnetic-dipole* polarization properties. These two transition regions are $^7F_0 \rightarrow {}^5D(3)_1$ (in the 527−529 nm part of the absorption spectra) and $^7F_1 \leftarrow {}^5D(3)_0$ (in the

592−596 nm part of the emission spectra). In all other transition regions, the observed lines are expected to exhibit predominantly *electric-dipole* polarization properties. The results obtained from our polarized absorption and emission measurements are entirely compatible with these expectations (*vide infra*).

Energy Level Analysis. The $4f^6$ electronic energy-level structure of Eu^{3+} in YbEuDPA was analyzed in terms of a model Hamiltonian defined to operate entirely *within* the $4f^6$ configuration, although it includes, in parametric form, some consideration of *interconfigurational mixings* (between $4f^6$ and higher-energy configurations of like parity). It is convenient to partition this Hamiltonian as follows:

$$\hat{H} = \hat{H}_a + \hat{H}_{cf}^{+} \tag{2}$$

where $\hat{H}_a$ is defined to incorporate the isotropic parts of $\hat{H}$ (including the spherically symmetric parts of the 4f-electron/crystal-field interactions) and $\hat{H}_{cf}^{+}$ is defined to represent the nonspherically symmetric components of the *even-parity* crystal field. We refer to $\hat{H}_a$ as the atomic Hamiltonian and call $\hat{H}_{cf}^{+}$ the *crystal-field* Hamiltonian. The explicit form of the $\hat{H}_a$ operator used in the present study is identical to that used in many previously reported analyses of $4f^N(Ln^{3+})$ energy-level structure. Here we write the $\hat{H}_a$ operator in the following parametrized form:

$$\hat{H}_a = E_{av} + \sum_k F^k \hat{f}_k + \alpha\hat{L}(\hat{L}+1) + \beta\hat{G}(G_2) + \gamma\hat{G}(R_7) + \sum_i T^i \hat{t}_i + \zeta_{so}\hat{A}_{so} + \sum_k P^k \hat{p}_k + \sum_j M^j \hat{m}_j \tag{3}$$

where $k = 2, 4, 6$; $i = 2, 3, 4, 6, 7, 8$; $j = 0, 2, 4$; and each of the interaction operators and parameters is written and defined according to conventional practice.[30,31] Defined according to eq 3, the $\hat{H}_a$ operator contains 20 parameters (including E_{av}). Implicit in these parameters are the radial-coordinate-dependent parts of the interactions represented in $\hat{H}_a$.

The even-parity crystal-field Hamiltonian, $\hat{H}_{cf}^{+}$, is defined to reflect the D_3 site symmetry of Eu^{3+} in YbEuDPA and is expressed here as

$$\hat{H}_{cf}^{+} = \sum_{k,m} B_m^k \hat{C}_m^{(k)} \tag{4}$$

where $k = 2, 4, 6$; $m = 0, \pm3, \pm6$ (with $|m| \le k$); $\hat{C}^{(k)}_m$ is an intraconfigurational spherical-tensor operator of rank k and order m; and the B_m^k are crystal-field interaction parameters. The B_m^k parameters in eq 4 are interrelated according to $B_{-m}^k = (-1)^m B_m^k$, and, therefore, this equation contains only six *independent* parameters.

Our energy-level calculations were carried out in two steps. In the first step the atomic Hamiltonian was diagonalized within the *complete set* of $f^6SM_SLM_L$ angular-momentum states (a total of 3003 states), with the parameters of $\hat{H}_a$ fixed at the values reported previously for Eu^{3+} in $Na_3[Eu(oda)_3]\cdot 2NaClO_4\cdot 6H_2O$. The 272 lowest-energy $f^6[SL]JM_J$ intermediate-coupled states derived from this calculation were then used as the basis set in our calculations of crystal-field energy-level structure. In these latter calculations, the *complete* model Hamiltonian ($\hat{H} = \hat{H}_a + \hat{H}_{cf}^{+}$) was diagonalized within the $f^6[SL]JM_J$ basis, with 16 of the 26 parameters in $\hat{H}$ treated as variables to fit calculated energy levels to experimentally observed energy-level data. Both the energies and symmetries of crystal-field levels were considered in performing these parametric data fits.

(30) Crosswhite, H. M.; Crosswhite, H. *J. Opt. Soc. Am. B* **1984**, *1*, 246.
(31) Carnall, W. T.; Goodman, G. L.; Rajnak, K.; Rana, R. S. *J. Chem. Phys.* **1989**, *90*, 3443.

Table 3. Energy Parameters for the $4f^6$ Electronic Configuration of Eu^{3+} in Hexagonal $Na_3[Yb_{0.95}Eu_{0.05}(dpa)_3]\cdot NaClO_4\cdot 10H_2O$

parameter[a]	value[b]/cm^{-1}	parameter[a]	value[b]/cm^{-1}
E_{av}	63 558(16)	M^0	4.25(0.40)
F^2	82 468(58)	M^2	$0.56M^0$
F^4	59 150(79)	M^4	$0.38M^0$
F^6	43 116(47)	P^2	647(91)
ζ_{so}	1336(1)	P^4	$0.75P^2$
α	20.2(0.2)	P^6	$0.50P^2$
β	−655(13)	B_0^2	−272(25)
γ	1336(12)	B_0^4	−103(52)
T^2	[370]	B_3^4	−433(29)
T^3	[40]	B_0^6	−483(67)
T^4	[40]	B_3^6	−1072(45)
T^6	[−330]	B_6^6	−812(41)
T^7	[380]		
T^8	[370]	N[c]	52
		σ[d]	9.8

[a] Defined according to eqs 3 and 4 in the text. [b] Determined from parametric fits of the experimentally observed energy-level data listed in Table 2. The numbers shown in parentheses represent uncertainties in the parameter values and correspond to the (±) changes in parameter values that produce a doubling of the *variance* obtained in the data fits. The parameter values shown in square brackets were held fixed in performing the data fits. [c] Number of assigned energy levels included in the parametric data fits. [d] Root mean square deviation between calculated and observed energies (cm^{-1}).

Transition Line Strengths. Line strengths were determined for 22 of the transitions observed in the low-temperature axial absorption spectra of YbEuDPA. Each of these transitions originates from the $A_1(^7F_0)$ *ground* level of Eu^{3+}, and they all terminate on excited crystal-field levels of E symmetry. The line strengths were determined from absorbance data according to eq 1 and the discussion that follows eq 1.

Direct calculations of *magnetic-dipole* line strengths were performed for both the $A_1 \rightarrow A_2$ and $A_1 \rightarrow E$ components of the $^7F_0 \rightarrow {}^5D(3)_1$ transition manifold *and* for both the $A_2 \leftarrow A_1$ and $E \leftarrow A_1$ components of the $^7F_1 \leftarrow {}^5D(3)_0$ transition manifold. The crystal-field state vectors required for these calculations were obtained as eigenvectors of the model Hamiltonian ($\hat{H}$) derived from the energy-level analysis described in the preceding section of this paper. These state vectors were used to evaluate the relevant magnetic-dipole transition moments and line strengths.

Results and Discussion

Crystal-Field Energy Levels. The energy levels located and assigned from our low-temperature optical absorption and emission measurements on single crystals of YbEuDPA are shown in Table 2, along with a listing of all *calculated* energy levels between 0 and 33 200 cm^{-1}. The levels are characterized with respect to their principal ^{2S+1}L-term and J-multiplet parentages, their crystal-field symmetry label ($\Gamma \equiv A_1$, A_2, or E) in the D_3 point group, and their observed and/or calculated energies. The calculated levels listed in Table 2 were obtained using the Hamiltonian parameter values shown in Table 3. The latter were derived from parametric fits of calculated-to-observed energy-level data, following the procedures described earlier. The number of observed levels included in these data fits was 52, and the number of Hamiltonian parameters allowed to freely vary in performing the data fits was 16. The M^2 and M^4 parameters and the P^4 and P^6 parameters were constrained according to the relationships shown in Table 3. The three-body configuration-interaction parameters T^i ($i = 2, 3, 4, 6, 7, 8$) were held fixed at the values shown in Table 3 (inside square brackets). The empirical data set was not sufficient to support a meaningful exploration of the T^i parts of the overall Hamiltonian parameter space.

Table 4. Comparison of Crystal-Field Interaction Parameters Reported for Eu^{3+} in Four Crystal Systems Having Trigonal Site Symmetries

parameter[a]	YbEuDPA(D_3)[b]	EuODA(D_3)[c]	EuES(C_{3h})[d]	Eu^{3+}:$LaCl_3$ (C_{3h})[e]
B_0^2	−272	67	118	193
B_0^4	−103	−839	−531	−296
B_3^4	−433	−692		
B_0^6	−483	−322	−574	−818
B_3^6	−1072	−810		
B_6^6	−812	−591	600	521
S_{cf}^2	122	30	53	86
S_{cf}^4	207	430	177	99
S_{cf}^6	544	403	284	305
S_{cf}	343	341	196	192

[a] The B_m^k crystal-field parameters are defined according to eq 4 in the text. The S_{cf}^k and S_{cf} *crystal-field strength* parameters are defined according to eqs 5 and 6 in the text. All parameter values are expressed in units of cm^{-1}. [b] From present work. [c] From ref 5 and J. Quagliano (University of Virginia), unpublished results. EuODA ≡ $Na_3[Eu(oda)_3]\cdot 2NaClO_4\cdot 6H_2O$. [d] From ref 34. EuES ≡ $[Eu(H_2O)_9](C_2H_5SO_4)_3$ ≡ europium nonahydrate tris(ethyl sulfate). [e] From ref 35.

The calculated results shown in Table 2 span the 30 lowest-energy [*SL*]*J* multiplet manifolds of $4f^6(Eu^{3+})$, and 21 of these multiplet manifolds are represented among the 52 crystal-field levels that were located and assigned from experiment. The $^3P(6)_0$, $^5F(2)_3$, and $^5F(2)_2$ multiplet manifolds are located at energies > 32 000 cm^{-1} (above ground), and absorptive transitions to these manifolds are obscured by broad and intense ligand absorption bands. Transitions to the $^5D(3)_3$, $^5L_8$, $^5L_9$, $^5L_{10}$, $^5H(1)_3$, and $^5H(1)_7$ multiplet manifolds are observed in the absorption spectra, but they are too weak to permit accurate characterizations of energy-level structure. The weakness of these transitions conforms to predictions based on ΔJ selection rules for both electric- and magnetic-dipole optical processes. For transitions that originate from the $^7F_0$(*ground*) level of Eu^{3+}, these selection rules are $\Delta J = 2$, 4, or 6 for electric-dipole processes and $\Delta J = 1$ for magnetic-dipole processes.

Hamiltonian Parameters. In Table 4, we show a comparison of the crystal-field interaction parameters determined for Eu^{3+} in four different trigonally symmetric systems. All of the crystal-field parameters (B_m^k) given in Table 4 are defined according to eq 4, with spherical-tensor normalization properties. Note, however, that the B_3^4 and B_3^6 parameters vanish in C_{3h} site symmetry. Also shown in Table 4 are the *crystal-field strength* parameters determined for Eu^{3+} in each of the host systems. These parameters are defined in terms of the B_m^k interaction parameters according to

$$S_{cf}^{\ k} = \left(\frac{1}{2k+1}[(B_0^{\ k})^2 + 2\sum_{m>0}|B_m^{\ k}|^2]\right)^{1/2} \quad (5)$$

$$S_{cf} = [^1/_3\sum_k (S_{cf}^{\ k})^2]^{1/2} \quad (6)$$

These strength parameters provide a measure of the extent to which the non-spherically symmetric components of the crystal-field interactions induce *J*-level mixings and shift the baricenter energies of *J*-multiplet manifolds.[32,33]

In each of the systems represented in Table 4 Eu^{3+} are located at 9-coordinate sites of trigonal symmetry, and in each system the coordination polyhedron formed by the nine ligand donor atoms about each Eu^{3+} ion has a slightly distorted tricapped trigonal prism structure. The Eu^{3+}-donor atom coordination clusters in the respective systems are: $Eu^{3+}(Cl^-)_9$ in Eu^{3+}:$LaCl_3$; $Eu^{3+}(O)_9$ in EuES ≡ $[Eu(H_2O)_9](C_2H_5SO_4)_3$; $Eu^{3+}(O^-)_6(O)_3$ in EuODA; and $Eu^{3+}(O^-)_6(N)_3$ in YbEuDPA. In both EuODA and YbEuDPA, the negatively-charged oxygen donor atoms are from ligand carboxylate groups and they are located at the vertices of the trigonal prismatic coordination polyhedron. The equatorial (prism-capping) coordination sites in EuODA are occupied by ether oxygen atoms (from $-CH_2OCH_2-$ ligand groups), and in YbEuDPA these coordination sites are occupied by pyridyl nitrogen atoms.

Table 5. Unpolarized Axial Line Strengths Determined for Absorptive Transitions Originating from the Ground Crystal-Field Level, A_1 ($^7F_0$), of Eu^{3+} in Hexagonal $Na_3[Yb_{0.95}Eu_{0.05}(dpa)_3]\cdot NaClO_4\cdot 10H_2O$

excited level[a]				
no.	multiplet	Γ	$\bar{\nu}^b$/cm^{-1}	axial line strength[c]
36	$^5D(3)_1$	E	18 951	0.6
37	$^5D(3)_2$	E	21 397	0.2
39	$^5D(3)_2$	E	21 433	7.6
46	$^5L_6$	E	24 930	12.4
52	$^5L_6$	E	25 189	79.8
54	$^5L_7$	E	25 926	0.5
58	$^5L_7$	E	26 060	1.1
63	$^5L_7$	E	26 163	0.3
66	$^5G(3)_3$	E	26 318	1.7
67	$^5G(3)_2$	E	26 355	1.7
68	$^5G(3)_2$	E	26 392	0.5
74	$^5G(3)_5$	E	26 493	1.1
79	$^5G(3)_6$	E	26 540	10.8
81	$^5G(3)_6$	E	26 563	4.6
83	$^5G(3)_5$	E	26 576	3.7
89	$^5G(3)_4$	E	26 655	1.5
108	$^5D(3)_4$	E	27 551	2.0
110	$^5D(3)_4$	E	27 561	2.2
158	$^5H(1)_4$	E	31 283	22.2
164	$^5H(1)_6$	E	31 386	15.2
168	$^5H(1)_6$	E	31 458	10.6
171	$^5H(1)_5$	E	31 520	4.2

[a] Identified according to the level-numbering and labeling scheme used in Table 2. [b] Observed wavenumber (corrected to vacuum) of the absorptive transition. [c] Line strength determined according to eq 1 of the text, assuming a Eu^{3+} concentration of 0.0962 M. Expressed in units of 10^{-6} D^2/χ_λ (see discussion following eq 1 in the text).

The results shown in Table 4 reveal striking differences between the 4f-electron/crystal-field interactions that contribute to the $4f^6(Eu^{3+})$ electronic energy-level structures in YbEuDPA and EuODA. This is apparent from the significant differences between the B_m^k (*and* S_{cf}^k) parameter sets determined for these two systems. We note, however, that the *overall* (total) crystal-field strength parameter, S_{cf}, is essentially identical for the two systems. This implies that the substitution of pyridyl for ether moieties in the three equatorial coordination sites about Eu^{3+} produces significant changes in the *anisotropies* of the 4f-electron/ligand-field interactions but does not alter the *overall interaction strengths*. The baricenter energies of the Eu^{3+} $4f^6$-[*SL*]*J* multiplet manifolds in YbEuDPA are essentially identical to those in EuODA, but the orderings and splittings of the crystal-field (Stark) levels *within* these manifolds are quite different in the two systems.

Absorption Line Strengths. The transition line strengths determined from our low-temperature axial absorption measurements on YbEuDPA are given in Table 5. Over the $^7F_0 \rightarrow {}^{2S+1}L_J$ (excited multiplet) transition regions surveyed in these measurements, which covered the 17 000−32 000 cm^{-1} spectral range, the most intense absorption lines were observed in the $^7F_0 \rightarrow {}^5L_6$ and $^7F_0 \rightarrow {}^5H(1)_{4,5,6}$ transition manifolds. This is similar to the findings reported previously for EuODA.[5] However, where line-by-line comparisons are possible, it is

(32) Leavitt, R. P. *J. Chem. Phys.* **1982**, *77*, 1661.
(33) Chang, N. C.; Gruber, J. B.; Leavitt, R. P.; Morrison, C. A. *J. Chem. Phys.* **1982**, *76*, 3877.
(34) Hammond, R. M. Ph.D. Dissertation, University of Virginia, 1988.
(35) Jayasankar, C. K.; Reid, M. F.; Richardson, F. S. *J. Less-Common Met.* **1989**, *148*, 289.

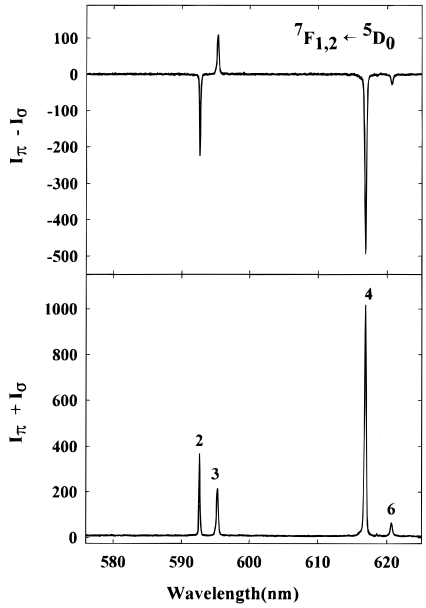

Figure 2. Spectra obtained from linearly polarized, orthoaxial emission measurements in the $^7F_{1,2} \leftarrow {}^5D(3)_0$ transition region of Eu^{3+} in hexagonal $Na_3[Yb_{0.95}Eu_{0.05}(dpa)_3]\cdot NaClO_4\cdot 10H_2O$ at 77 K. The sum ($I_\pi + I_\sigma$) and difference ($I_\pi - I_\sigma$) intensity scales are expressed in identical, but arbitrarily chosen, units. See text for a description of the line-numbering scheme.

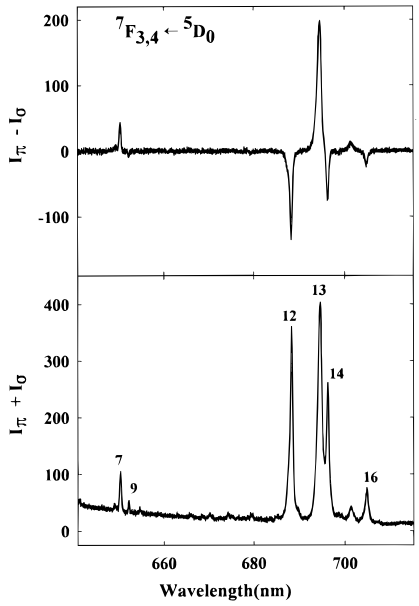

Figure 3. Spectra obtained from linearly polarized, orthoaxial emission measurements in the $^7F_{3,4} \leftarrow {}^5D(3)_0$ transition region of Eu^{3+} in hexagonal $Na_3[Yb_{0.95}Eu_{0.05}(dpa)_3]\cdot NaClO_4\cdot 10H_2O$ at 77 K. The sum ($I_\pi + I_\sigma$) and difference ($I_\pi - I_\sigma$) intensity scales are expressed in identical, but arbitrarily chosen, units. See text for a description of the line-numbering scheme.

observed that the 4f → 4f transition intensities in YbEuDPA are generally somewhat stronger than those in EuODA. This applies to essentially all of the predominantly *electric-dipole* transitions, but not to the predominantly *magnetic-dipole* $^7F_0 \rightarrow {}^5D(3)_1$ transitions. The latter show comparable line intensities in YbEuDPA and EuODA.

The axial line strength determined for the $A_1 \rightarrow E$ component of the $^7F_0 \rightarrow {}^5D(3)_1$ transition in YbEuDPA is 0.6×10^{-6} D^2. This experimentally observed line strength is reasonably well-predicted by direct calculations that assume a pure magnetic-dipole transition mechanism. The line strength obtained from these direct calculations is 0.76×10^{-6} D^2.

The line-strength values given in Table 5 were determined from absorbance data according to eq 1, with the concentration of Eu^{3+} in our YbEuDPA crystal samples assumed to be 0.0962 mol/L. This assumed concentration of Eu^{3+} corresponds to that expected for crystals of stoichiometric formula $Na_3[Yb_{0.95}Eu_{0.05}(dpa)_3]\cdot NaClO_4\cdot 10H_2O$, which, in turn, reflects the mole percent ratio of Yb^{3+} to Eu^{3+} in the crystal-growth solution. As was discussed earlier in the paper, the *actual* concentration of Eu^{3+} ions in the crystal samples is estimated to be within ±20% of the 0.0962 mol/L value used in our line-strength calculations.

Polarized Emission Spectra. Figures 2−4 show spectra obtained from linearly polarized emission measurements performed on single crystals of YbEuDPA at 77 K. These spectra span the $^7F_J(J=0-6) \leftarrow {}^5D(3)_0$ transition regions of Eu^{3+}, and the peak (or line) numbers shown in these spectra identify the *terminal* crystal-field levels involved in individual transitions (see Table 2 for the energy-level numbering scheme). The locations and polarization properties observed for a subset of the emission lines are given in Table 6.

Note from the spectra shown in Figure 2 that no emission lines are observed in the $^7F_0 \leftarrow {}^5D(3)_0$ transition region (predicted to be located near 580 nm). This conforms with the electric- and magnetic-dipole selection rules given in Table 1 for an $A_1 \leftarrow A_1$ type transition in $Eu(dpa)_3^{3-}$ complexes that have trigonal-dihedral (D_3) symmetry.

Emission Excitation Spectra. The emission excitation spectra of YbEuDPA generally mimic the spectra obtained from direct optical absorption measurements with respect to both the

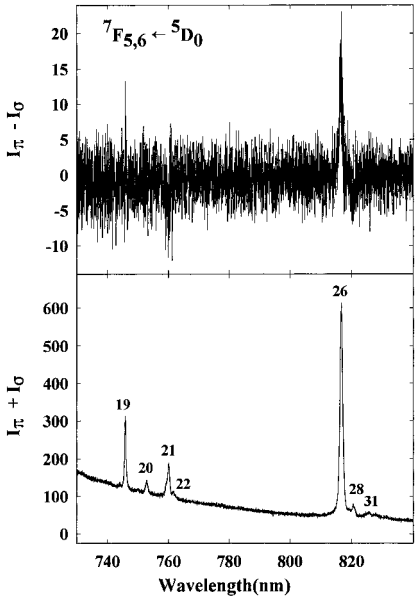

Figure 4. Spectra obtained from linearly polarized, orthoaxial emission measurements in the $^7F_{5,6} \leftarrow {}^5D(3)_0$ transition region of Eu^{3+} in hexagonal $Na_3[Yb_{0.95}Eu)_{0.05}(dpa)_3]\cdot NaClO_4\cdot 10H_2O$ at 77 K. The sum ($I_\pi + I_\sigma$) and difference ($I_\pi - I_\sigma$) intensity scales are expressed in identical, but arbitrarily chosen, units. See text from a description of the line-numbering scheme.

locations and polarization properties of transitions. However, the detection limits achievable in the emission excitation experiments are somewhat superior to those in the direct absorption measurements, and a few more lines are observed in the emission excitation spectra. Most of the "extra" lines observed in the excitation spectra correspond to very weak *one-phonon vibronic* transitions with well-defined origins. However, a few $A_1 \rightarrow A_1$ type *origin* transitions also appear when the excitation spectra measurements are pushed to the detection limits of our instrumentation. This is illustrated in Figure 5, where an excitation scan through the $^7F_0 \rightarrow {}^5D(3)_0$ transition region of Eu^{3+} is shown. The spectrum in Figure 5 was obtained with laser excitation along the *c*-axis of a YbEuDPA crystal

Table 6. Polarizations of Emission Lines Observed in the $^7F_J(J=1,2,3,4) \leftarrow {}^5D_0$ Transition Regions of Eu^{3+} in Hexagonal $Na_3[Yb_{0.95}Eu_{0.05}(dpa)_3]\cdot NaClO_4\cdot 10H_2O$

terminal level[a]				
no.	multiplet	Γ	$\bar{\nu}^b/cm^{-1}$	P^c
2	$^7F_1$	A_2	16 869	0.62
3	$^7F_1$	E	16 794	−0.52
4	$^7F_2$	E	16 206	0.49
6	$^7F_2$	E	16 109	0.50
7	$^7F_3$	A_2	15 370	−0.57
9	$^7F_3$	A_2	15 328	0.23
12	$^7F_4$	E	14 524	0.39
13	$^7F_4$	A_2	14 392	−0.49
14	$^7F_4$	E	14 358	0.29
16	$^7F_4$	E	14 185	0.29

[a] Identified according to the level-numbering and labeling scheme used in Table 2. In all cases, the emitting level is A_1 ($^5D_0$). [b] Observed wavenumber (corrected to vacuum) of the emissive transition. [c] Transition polarization defined by $P = (I_\sigma - I_\pi)/(I_\sigma + I_\pi)$, where I_σ and I_π denote σ-polarized and π polarized emission intensities obtained in orthoaxial spectral measurements.

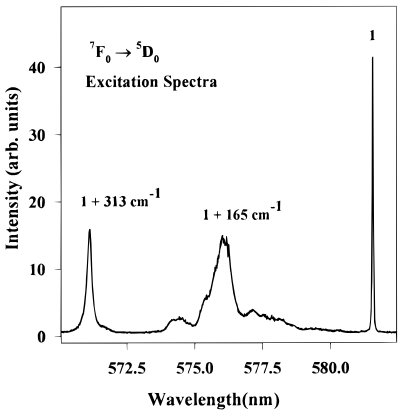

Figure 5. Emission excitation spectrum in the $^7F_0 \rightarrow {}^5D(3)_0$ transition region of Eu^{3+} in hexagonal $Na_3[Yb_{0.95}Eu_{0.05}(dpa)_3]\cdot NaClO_4\cdot 10H_2O$ at 77 K. Emission intensity was monitored at 617 nm.

sample (at 77 K), and with sample emission intensity monitored at 617 nm. The very sharp line located at 581.5 nm (and labeled as 1) in the $^7F_0 \rightarrow {}^5D(3)_0$ excitation spectrum is assigned to the erstwhile $A_1 \rightarrow A_1$ electronic origin transition, and the remaining lines and spectral features are assigned to one-phonon vibronic transitions. The latter are located at the following wavenumber displacements from the origin line: 100, 110, 119, 131, 165, 175, 183, 213, and 313 cm^{-1}. Note from Figure 5 that the total integrated intensity of the vibronic transitions is considerably greater than that of the electronic origin transition.

Detection of the $^7F_0 \rightarrow {}^5D(3)_0$ origin transition in the excitation spectrum of YbEuDPA indicates at least some small distortion of the Eu^{3+} sites away from exact trigonal-dihedral (D_3) symmetry. However, evidence for this distortion appears only in the excitation spectra, and it is clear that *either* the distortion is very slight *or* the number of distorted sites is very small. The direct absorption and emission spectra measurements performed on YbEuDPA do not reveal any detectable deviations from the D_3-symmetry-based selection rules shown in Table 1.

Comparisons between Single-Crystal and Solution-Phase Results. Both optical excitation and emission measurements have been reported in the literature for $Eu(dpa)_3^{3-}$ complexes in neutral aqueous solution at room temperature.[1,26,27] The solution-phase emission measurements spanned all of the $^7F_J \leftarrow {}^5D(3)_0$ transition regions examined in the present study, but the excitation spectra measurements were confined to the $^7F_{0,1} \rightarrow {}^5D(3)_{0,1,2}$ transition regions. Comparisons between the room-temperature spectra obtained for $Eu(dpa)_3^{3-}$ in YbEuDPA and in aqueous solution indicate essentially identical $4f^6(Eu^{3+})$ energy-level structures in the two (crystalline and solution) media. Furthermore, the relative intensities observed among the different *J*-multiplet-to-*J*-multiplet transition manifolds (in the emission and excitation spectra) are essentially identical for $Eu(dpa)_3^{3-}$ in YbEuDPA and in solution. Comparisons of relative line intensities *within J*-multiplet-to-*J*-multiplet transition manifolds also indicate that the optical properties of $Eu(dpa)_3^{3-}$ are essentially the same in YbEuDPA and in solution.

In the $^7F_1 \leftarrow {}^5D(3)_0$ emission region of $Eu(dpa)_3^{3-}$ in aqueous solution, the $E \leftarrow A_1$ and $A_2 \leftarrow A_1$ transition components exhibit an intensity ratio of 2.3. This observed ratio is reasonably close to that predicted, 2.0, from direct calculations based on the crystal-field state vectors derived from our YbEuDPA energy-level analysis. In the $^7F_0 \rightarrow {}^5D(3)_1$ excitation region of $Eu(dpa)_3^{3-}$, the calculations predict an intensity ratio of 1.4 for the $A_1 \rightarrow E$ versus $A_1 \rightarrow A_2$ component transitions, which may be compared to an observed ratio of 1.5.

Finally, we note that the *chiroptical* properties of $Eu(dpa)_3^{3-}$ in solution may be studied by using a combination of circularly polarized excitation *and* emission measurement techniques.[24,26,27] In these studies, circularly polarized light is used to preferentially excite either the Λ or Δ enantiomeric forms of $Eu(dpa)_3^{3-}$, and circularly polarized emission is then observed from the resulting nonracemic excited-state population of complexes. In principle, these same circularly polarized excitation/emission measurement techniques should be applicable to the racemic mixture of Λ-$Eu(dpa)_3^{3-}$ and Δ-$Eu(dpa)_3^{3-}$ complexes present in YbEuDPA. However, so far we have not been able to observe any circularly polarized emission from YbEuDPA samples excited with circularly polarized light. One possible explanation for this is that excited-state energy-transfer processes between Λ-$Eu(dpa)_3^{3-}$ and Δ-$Eu(dpa)_3^{3-}$ complexes in the crystal samples are fast on the $^5D_0$ emission time scale. However, this explanation seems unlikely given the low concentration levels of Eu^{3+} in our YbEuDPA ≡ $Na_3[Yb_{0.95}Eu_{0.05}(dpa)_3]\cdot NaClO_4\cdot 10H_20$ crystal samples. It remains unclear why a nonracemic excited-state population of $Eu(dpa)_3^{3-}$ complexes cannot be detected in YbEuDPA samples excited with circularly polarized light.

Conclusion

In this study, a combination of polarized and unpolarized optical absorption and emission measurements were used to locate and assign 52 of the crystal-field energy levels split out of the $4f^6(Eu^{3+})$ electronic configuration in tris(dipicolinate)-europium(III) complexes. The energy-level data obtained from these measurements were analyzed in terms of a model Hamiltonian constructed to represent the major interactions that contribute to the $4f^6$ electronic state structure of Eu^{3+} in $Eu(dpa)_3^{3-}$. This analysis yielded interaction parameters that provide information about both the anisotropies and the overall strength of the contributing 4f-electron/ligand-field interactions, and the values obtained for these interaction parameters were compared to those determined for Eu^{3+} in several other systems. Optical line strengths were determined for 22 of the Stark-level-to-Stark-level transitions observed in the low-temperature axial absorption spectra of $Eu(dpa)_3^{3-}$ in single crystals of $Na_3[Yb_{0.95}Eu_{0.05}(dpa)_3]\cdot NaClO_4\cdot 10H_2O$.

Comparisons between the results obtained in the present study and those reported in previous work indicate that the $4f^6(Eu^{3+})$ electronic energy-level structure of $Eu(dpa)_3^{3-}$ in $Na_3[Yb_{0.95}Eu_{0.05}(dpa)_3]\cdot NaClO_4\cdot 10H_2O$ is essentially identical to that of $Eu(dpa)_3^{3-}$ in neutral aqueous solution.

Acknowledgment. This work was supported by the U.S. National Science Foundation (NSF Grant CHE-9213473 to F.S.R.).

IC951524G